A Study Toward Device Development for Nano-Enabled Microwave Water Treatment

by

Sneha Siddharth Jain

Honors Thesis

Presented to the

Engineering Honors Program

The University of Texas at Austin

in Partial Fulfillment

of the Requirements

for the Degree of

Bachelor of Science in Chemical Engineering

The University of Texas at Austin

May 2019

Abstract

A Study Toward Device Development for Nano-Enabled Microwave Water Treatment

Sneha Siddharth Jain

The University of Texas at Austin, 2019

Supervisor: Dr. Navid B. Saleh

In the United States, while regulations for clean water exist, many community-based water systems frequently violate standards for water quality. Of these violations, a large component arises from coliform bacteria. Existing treatment methods suffer from high monetary cost, long bacterial inactivation time, low equipment availability, and/or generation of byproducts in bacterial inactivation. In this study, microwave irradiation of carbon nanotubes will be harnessed for a low-cost, convenient bacterial inactivation method for water treatment. The device developed harnesses conventional microwave ovens' high market penetration, even among lower income strata, and carbon nanotubes' exceptional mechanical, electronic, and thermal properties. Microwave irradiation of carbon nanotubes allows for rapid, uniform heating, which holds promise for rapid bacterial inactivation. A plaster of Paris and cement matrix was formed using sugar as a pore-forming agent; varying quantities of multi-wall carbon nanotubes of varying oxidation levels were incorporated in the device preparation. The heating response for each treatment in 1 mL of water was observed for microwave irradiation ranging from 30 s to 3

min and 30 s, in intervals of 30 s. Results demonstrate incorporation of multi-wall carbon nanotubes provide a rapid heating response at 5% of device weight. Pristine MWCNTs have a more rapid heating behavior and higher temperature achieved than other treatments, suggesting that defects and functionalization have a negative impact on the heating behavior. Nonetheless, all treatments appear to plateau, implying that saturation of the MWCNTs' heating abilities can occur. These initial results are promising, but much work remains in optimizing and verifying device characteristics.

Table of Contents

List of Figures

List of Tables

List of Symbols and Abbreviations

1-D	One-dimensional
CNT	Carbon nanotube
DI	Deionized
DLS	Dynamic light scattering
fCNT	Functionalized carbon nanotube
fMWCNT	Functionalized multi-wall carbon nanotube
HRTEM	High-resolution transmission electron microscopy
MW	Microwave
MWCNT	Multi-wall carbon nanotube
NM	Nanomaterial
NP	Nanoparticle
OD	Outer diameter
PP	Plaster of Paris
SWCNT	Single-wall carbon nanotube
XPS	X-ray photoelectron spectroscopy

Section 1: Introduction

1.1 Motivation

Although commonly considered a problem solely in developing nations, water quality and treatment are important considerations even in developed nations. Allaire, Wu, and Lall[1], through analyzing panel data of 17,900 community water systems in the continental United States, demonstrate that violations are widespread across the country, affecting 9-45 million individuals (4-28% of the population) yearly, most notably in rural areas. Though violations may be infrequent, consistent access to safe water is a necessity.

The water treatment process can involve many steps, including pre-chlorination, aeration, coagulation, sedimentation/filtration, and disinfection, for the purpose of arresting biological growth, removing heavy metals, removing foreign solids and liquids, and inactivating pathogens. As the most prevalent violation in Allaire et al.'s study was total coliform bacteria, representing 37% of the reported violations[1], the focus of study towards water treatment will be constrained to bacterial inactivation. Figure 1 illustrates the geographic distribution of total coliform violations over a period of 33 years.

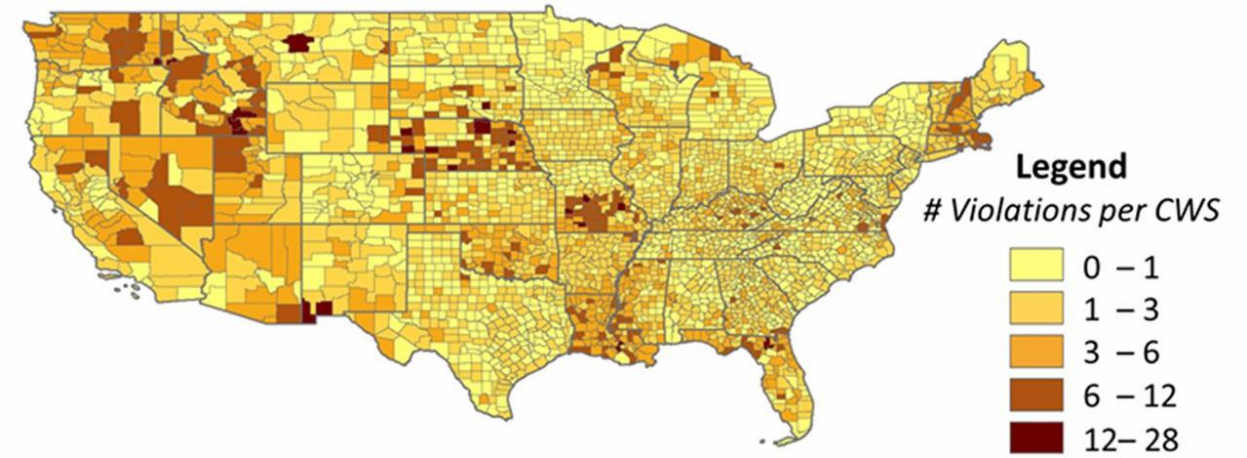

Figure 1: Number of total coliform violations per CWS, 1982–2015, by county[1].

Table 1: Comparison of point-of-use bacterial inactivation methods.

	Expense	Time	Availability	Byproducts	Other
Boiling	+	-	+	+	• Concentration of heavy metals • Does not remove pollutants • Not all pathogens inactivated at 100 °C
UV Irradiation	-	+	-	+	• Requires UV lamp • Inhibits bacterial reproduction • Poor effectiveness in turbid solutions • Can be reversed by photoactiviation
Reverse Osmosis	-	-	-	+	• Requires pressurized system • Much waste water generated • Removes pathogens, contaminants, and salts depending on size and membrane selectivity
(Solar) Distillation	+	-	+	+	• Removes all pathogens, contaminants, and salts
Activated Carbon Filtration	0	+	+	+	• Viruses and small bacteria retained • Filter can become colonization site • Adsorbs many toxic compounds
Iodine	+	0	+	-	• Ascorbic acid required to alter taste and precipitate iodine • Incomplete effectiveness against *Cryptosporidium* and *Giardia*
Bleach	+	0	+	-	• Incomplete effectiveness against *Cryptosporidium* and *Giardia*

Note: + corresponds to a positive attribute, 0 to a neutral attribute, and - to a negative attribute.

Feasibility of current point-of-use bacterial removal devices are assessed in Table 1. Considerations include expense, time, availability of materials, byproduct generation, and other characteristics. Certain bacteria may be resistant to UV irradiation, iodine, and/or bleach. The use of iodine or bleach can also introduce toxic byproducts, while boiling can concentrate contaminants. Other promising solutions are stymied by availability, cost, and convenience.

Microwave irradiation can prove useful for water treatment due to the prevalence of domestic microwave ovens. Of American households, 96.8% overall own a microwave; even among the lowest income quintile, 93.4% own a microwave[2]. While a low-energy method, microwave ovens are able to deliver sufficient heat to boil water.

To compound microwave heating, nanomaterials can be implemented. With high surface area-to-volume ratios, nanomaterials can be used to improve heating with only small quantities necessary, allowing them to be a potentially cost-effective option. Carbon nanotubes display excellent thermal, electrical, and structural properties. Upon microwave irradiation, carbon nanotubes exhibit a rapid and uniform heating behavior that can prove useful to bacterial inactivation. Nanotube modification can also permit reactive oxygen species generation, which can damage cell structures by oxidative stress.

In order to contain the nanomaterials, the carbon nanotubes can be held in a ceramic matrix. Such a structure should retain its shape in aqueous environments, contain the nanomaterials, and contain pores to allow for greater surface contact with the carbon nanotubes and permit flow through applications.

In this thesis, the microwave absorption-potential of carbon nanotubes is exploited towards a novel point-of-use bacterial inactivation method for water treatment. Multi-wall carbon nanotubes were incorporated into plaster of Paris-based matrices. Heating behavior was

observed for carbon nanotubes of varying degrees of oxidation at various loadings. Results obtained in this study demonstrate the enhanced heating behavior nano-enabled devices can effect and serve as a novel application of microwave irradiation of carbon nanotubes.

1.2 Objectives and Hypotheses

The primary objective of this study is to develop multi-wall carbon nanotube-enabled porous devices for use in batch bacterial inactivation of water. The hypothesis that the extent of functionalization on multi-wall carbon nanotubes will influence extent of interfacial heating to potentially enhance water treatment of such devices will be tested.

The following sub-objectives and corresponding hypotheses inform the experimental design:

Objective 1. Perform a literature review to understand the properties of carbon nanotubes and derivative materials.

Objective 2. Develop a PP matrix to immobilize carbon nanotubes.

Objective 3. Vary degree of heating caused by devices.

Hypothesis: Amount and extent of functionalization of CNTs on the PP matrix will modulate surface heating.

1.3 Thesis Structure

This thesis will follow a structure aligning to the objectives.

Section 2: Multifunctional Properties of CNTs

Defines and characterizes CNTs, with specific attention devoted to modified multi-wall carbon nanotubes and effect of microwave irradiation.

Section 3: CNT Functionalization and Characterization

Outlines MWCNT functionalization process and assesses aggregation behavior and composition of products.

Section 4: Device Development and Microwave Irradiation

Presents design of devices and aqueous assesses heating behavior upon microwave irradiation

Section 5: Conclusions and Recommendations

Summarizes major findings of the study and provides recommendations for future study

Section 2: Multifunctional Properties of CNTs

2.1 INTRODUCTION

Carbon nanotubes are a 1-D allotrope of carbon, often described as rolled graphene sheets. The carbon atoms are bonded together in the sp^2 configuration, resulting in a stable structure. While nanotube diameter is in the nanometer range, length can vary widely, though typically in the micrometer or millimeter range. The length-to-diameter aspect ratio[3] can reach up to 1.32×10^8:1, significantly higher than that of other materials. Chirality, or the direction of rolling, is another defining characteristic that describes the symmetry of rolling.

The chemical properties of carbon nanotubes rely on three factors[4]:

Factor 1: sp^2 hybridization of the carbon atoms and the distortion of these hybrid orbitals due to curvature-induced strain

Factor 2: π orbital misalignment between adjacent carbon atom pairs

Factor 3: sp^3 defects

Following from Factor 1, carbon nanotubes extend many of the properties of graphene sheets. Graphene is metallic (in-plane), stiff, and a good conductor of thermal energy. Similarly, the strong C=C bonds in CNTs also result in a high elastic modulus and high thermal conductivity. Electrical conductivity, however, varies based on diameter and/or chirality, which are interrelated factors, yielding either metallic or semiconducting behaviors, as per Factors 1 and 2.

Concentric nesting of nanotubes produces multi-wall carbon nanotubes (MWCNTs), as opposed to single-wall carbon nanotubes (SWCNTs). Each tube in a MWCNT is separated by 0.340 nm, and the nesting of multiple nanotubes contributes to a larger outer diameter than SWCNTs, which results in lower reaction affinity[4]. MWCNTs also have a lower thermal

conductivity than SWCNTs due to quenching on phonon modes and weak transport at tube-tube junctions and curvature effects induce MWCNTs to be stiffer than SWCNTs.

2.2 PROPERTIES OF MULTI-WALL CARBON NANOTUBES

The following discussion will focus on MWCNTs, as they were used in this study. MWCNTs appear as a low density[4] (0.03 g/cm^3 to 0.22 g/cm^3) fluffy black powder.

Pristine MWCNTs have low solubilities and do not disperse well in water due to high van der Waals and electrostatic interactions. Increased solubility can be achieved through shortening nanotubes, surface functionalization, and/or use of surfactant; for example[4], untreated MWCNTs may be dissolved up to 0.05 mg/mL in water, while carboxy-functionalized MWCNTs may be dissolved up to 0.5 mg/mL in water.

Mechanically, MWCNTs have excellent properties. In the axial direction, the elastic modulus[5] is in the TPa range and tensile strength[6] is 60 GPa; in the radial direction, the nanotubes are comparatively weaker, with an elastic modulus[7] of 30 GPa, which makes them relatively easy to mechanically modify. Due to the ultralow friction[8] (less than 1.4×10^{-15} N/atom) between MWCNT walls, the outermost shell is the only load-bearing element of the MWCNT[9]. Although defects reduce individual wall strength, they improve the load transfer between the walls[10].

The outermost wall, additionally, determines electronic properties of MWCNTs at low bias and low temperature by its chirality[11,12,13]. Inner walls may exhibit different chirality, though are nonnegligible in their effect on lowering MWCNT resistance[14,15]. MWCNTs have electrical current conductivity in the magnitude of 10^4 to 10^5 S/m, depending on the synthesis and treatment method[16]. They can also support high current densities and high temperatures, with current density[17,18,19] ranging from 10^6 to 10^8 A/cm^2, even at 3200 K. Semiconducting CNTs

have a significantly high engineered bandgap variation, ranging from 20 meV to 2 eV, with bandgap increasing inversely proportional to diameter[20]. Band structure modulation can also be effected by application of electric and magnetic fields.

With respect to thermal properties, the configuration of the MWCNT network greatly affects the performance. The effective average thermal conductivity[21] of MWCNTs is 200 W/(mK), with measured data[22] indicating conductivities between 180 and 220 W/(mK). Individual MWCNTs, however, provided thermal conductivities around 650-830 W/(mK) and over 3000 W/(mK) for supported[23] and free-standing/suspended[24] MWCNTs, respectively, at room temperature. The lower network thermal conductivity could be a result of strong intertube coupling[25]. A suspension of 0.6 vol-% MWCNTs in water increased the thermal conductivity of water[26] by up to 38%.

2.3 Carbon Nanotube Modification

Pristine carbon nanotubes' excellent properties can be further exploited through modification. Broadly, CNTs' properties can be extended with functional groups and/or substrates attached to the material. Hybrids can be formed from a variety of adducts, including DNA[27,28], proteins[29], enzymes[30,31], dyes[32], polymers, surfactants, metallic nanoparticles, and semiconducting quantum dots. Such modification can take place through three processes: doping, defect introduction, and functionalization.

Doping incorporates of foreign matter into or on the nanotube surface. There are three categories. (1) Exohedral doping or intercalation occurs when heteroatoms or functional groups covalently or noncovalently attach to the nanotube surface. Due to surface reactivity, exohedral doping is more common than endohedral doping. (2) In endohedral doping or encapsulation, heteroatoms or structures fill the MWCNT core. (3) In-plane or substitutional doping involves

one or more heteroatoms covalently added to the nanotube lattice. The aforementioned chemical doping methods tune the Fermi energy level of CNTs in either the conduction band or the valence band; note that at normal atmosphere and room temperature, semiconducting CNTs are p-type due to the inherent curvature that results in self-doping[33]. Some doping may arise through the nanotube synthesis method.

Defects may also take multiple forms. Structural defects are pentagons, heptagons, and/or octagon carbon rings embedded in the sp^2 lattice that significantly modify the overall curvature. Modified carbon ring structures that do not significantly alter the overall curvature comprise topological defects or bond rotations; these may notably be 5-7-7-5 pairs or Thrower-Stone-Wales defects creating by bond rotation two pentagons and two heptagons[34,35]. Tube radial change has not been studied in detail, and further non-sp^2 carbon defects may also rise from reactive carbon atoms as interstitials, edges, and adatoms.

Functionalization is often considered to improve dispersion in aqueous solutions or to create polymer composites to exploit the enhanced electrical and mechanical properties CNTs can offer. Modification may be covalent, through π-π interactions, or electrostatic.

A common process for covalent functionalization is oxidation and subsequent derivatization. Sonication in strong acids[i] can remove unwanted carbonaceous materials, shorten nanotubes, and introduce oxygen-based functional groups. The functionalities arise primarily at the ends of nanotubes and sites of increased reactivity, such as defect sites, but also along sidewalls[36]. The carboxyl functional groups readily allow for open nucleophilic chemistry for hybridization[4]. Fluorination, aryl diazonium chemistry, and nitrenes can also form functional

[i] Note that sonication in water can also create oxygen-containing functional groups (hydroxide, carbonyl, carboxyl). See Yang, D.-Q., Rochette, J.-F., & Sacher, E. (2005). Functionalization of Multiwalled Carbon Nanotubes by Mild Aqueous Sonication. *The Journal of Physical Chemistry B, 109*(16), 7788–7794. doi:10.1021/jp045147h

groups on CNTs. These methods of covalent functionalization can significantly alter the desirable properties of carbon nanotubes.

π-π interactions involve stacking of nonpolar molecules (with aromatic rings or C=C bonds) near the surface of carbon nanotubes. The location and orientation of the nonpolar molecule is such that the σ-π attractive interactions are maximized and the π-π repulsive interactions are minimized. Polymer wrapping is an extension of this functionalization, involving molecules with large π systems.

Electrostatically functionalized CNTs are first modified to create active sites and subsequently derivatized with molecules with high charge density. Electrostatic interactions, in contrast to covalent bonding as in covalent functionalization, binds polyelectrolytes, DNA, proteins, metallic NPs, etc. to CNT surfaces.

Modified CNTs may be characterized in several ways; a select few are described here.

Transmission Electron Microscopy (TEM)

High resolution transmission electron microscopy allows direct observation of nanotube walls. With sufficient magnification and resolution, crystallinity and defects can be observed through wall straightness, variations in local curvature, tubular deformation, variation in wall spacing, etc. Hybridized materials, their size, and their distribution may also be visually observed.

X-ray photoelectron spectroscopy (XPS)

X-ray photoelectron spectroscopy (XPS) is a procedure through which a focused beam of x-rays irradiates the surface of a sample and the kinetic energy of escaping electrons is measured. XPS permits quantitative determination of bond types for the surface of a material (up to 20 nm in depth) through peak fitting. Crystallinity can be measured through comparing the sp^2 C=C

(284.3 eV) bonding and the sp^3 C-C (285.2 eV) bonding. In oxidized samples, the C-O (286.5 eV), C=O (287.3 eV), -COO (288.8 eV), O-C=O (288.5 eV), and O-COO (290.3 eV) bonds may be monitored in the C1s region and the O=C (531.7 eV), O-C (533.3 eV), and O-COO (534.4 eV) bonds in the O1s region[37]. Note that Auger emission may also occur, in which an electron ejected from the 1s state (K shell) is filled by an electron from the L shell and another electron from the L shell is ejected[38].

Raman Spectroscopy

In Raman spectroscopy, incident laser light is used to observe vibrational, rotational, and other low-frequency modes of a system. Excited electrons jump from the valance band to the conduction band after adsorbing photons and may scatter through emission or absorption of phonons. As an electron relaxes, it emits a photon, which is recorded by a detector, with background and elastic scattering filtered out.

For MWCNTs, the Raman spectrum is predominantly characterized by two peaks. At 1590 cm^{-1}, the *G* mode describes tangential stretching C-C vibrations in the nanotube wall plane[4]. The *D* mode, at 1350 cm^{-1}, describes the double resonance process attributed to amorphous disordered carbon, covalent modification, and defects[4,39]. Acid treatment as a process of functionalization exerts pressure on the tube[ii], such that the *D* and *G* bands are upshifted[39].

While the *D* band is not specific to measuring defects, comparing the *D* and *G* band intensity (I_D and I_G, respectively) is an accepted measure for general purity of MWCNT samples[4]. Osswald et al., further, demonstrated that oxidation removes amorphous carbon from the CNT surface, such that the D band would be indicative of modification and defects for oxygen-functionalized MWCNTs[40]. Although Murphy et al.[39] and DiLeo, Landi, and Raffaelle[41]

[ii] Note, however, it is difficult to separate the effects of electron transfer and those of strain in the acid-functionalized MWCNTs.

argue that in lieu of I_D/I_G, a measure containing the defect-independent[42] second order overtone mode *D** is more appropriate due to the convolution of the *G* and *D'* modes, the latter of which is impacted by the defect induced, double resonance process, the I_D/I_G measure will be used due to convention.

Additional characterization methods include atomic force microscopy, scanning transmission microscopy, electron energy loss spectroscopy, and thermogravimetric analysis.

2.4 Carbon Nanotube Responses to Microwave Irradiation

The microwave band of radiation is defined as electromagnetic waves with frequencies between 300 MHz and 300 GHz; for industrial and domestic use, the main operational frequency[43] is 2.450 (+/- 0.050) GHz.

Microwaves are often exploited for their heating properties. Haque[44] finds microwave heating is advantageous compared to conventional heating, as it offers non-contact heating, energy transfer in lieu of heat transfer, rapid heating, material selective heating, volumetric heating, quick start-up and stopping, heating from the interior of the material body, and a higher level of safety and automation. Paton and Windle[45] add that microwave heating exhibits higher throughput, greater penetration depth of heat into material, and lower power costs.

This heating behavior is a result of conduction and dielectric heating[iii], expressed by a dielectric constant (real permittivity) and a dielectric loss factor (imaginary permittivity), measuring absorbance of incident energy and dissipation, respectively[46]. Dielectric heating arises from the interaction of charged particles and high-frequency radiation. Permanent and induced

[iii] Note the contribution of magnetic heating becomes small at the microwave range as per Snoek's law. See Qin, F., & Brosseau, C. (2012). A review and analysis of microwave absorption in polymer composites filled with carbonaceous particles. *Journal of Applied Physics*, *111*(6), 061301. doi:10.1063/1.3688435 and Snoek, J. L. (1948). Dispersion and absorption in magnetic ferrites at frequencies above one Mc/s. *Physica*, *14*(4), 207–217. doi:10.1016/0031-8914(48)90038-x

dipoles in polar materials rotate in the alternating field, generating friction and heat. Alternatively, in dielectric solid materials with mobile charged particles, a current is induced, which dissipates as heat due to the Maxwell-Wagner effect[43]. Carbon materials have a high capacity to absorb and convert microwave energy into heat due to their high dielectric loss tangent (0.25-1.14 for carbon nanotubes compared to 0.118 of distilled water).

The interaction between carbon nanotubes and microwave irradiation is of growing recent interest. Figure 2 tracks annual publications and citations for articles pertaining to carbon nanomaterial and carbon nanotube microwave absorption. Publications have experienced modest growth; however, citations have increased fourfold for carbon nanotubes and fivefold for carbon nanomaterials in the past decade.

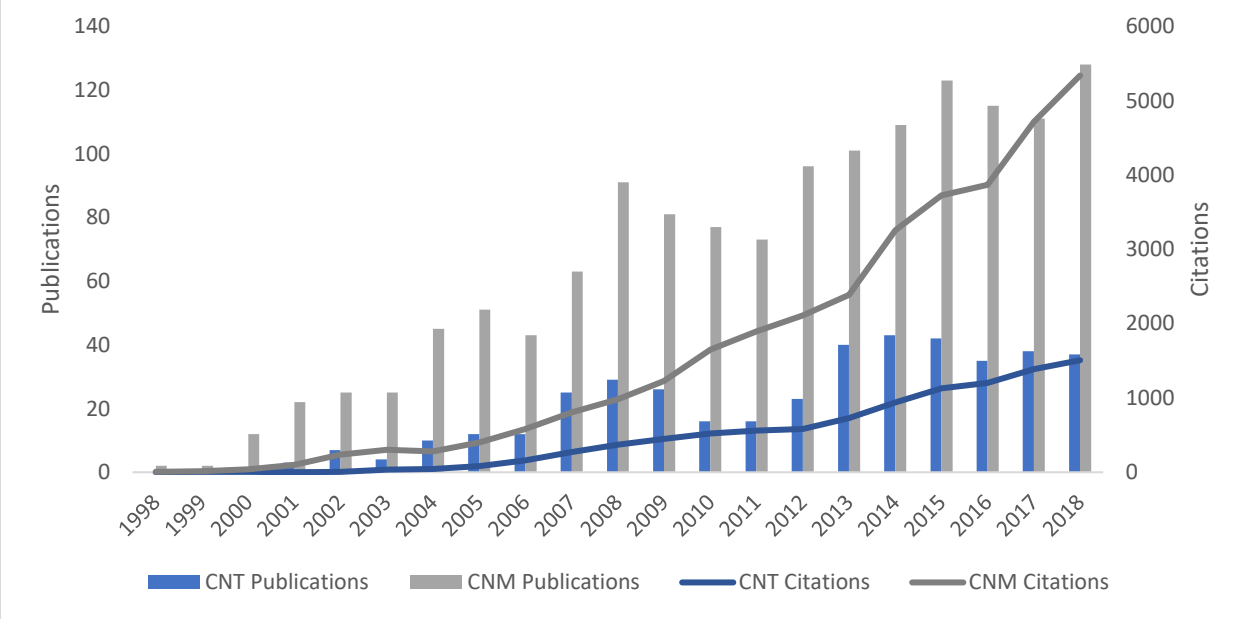

Figure 2: Annual publications and citations for microwave irradiated carbon nanotubes (CNT) and carbon nanomaterials (CNM) in the Web of Science®[iv]

[iv] Search criteria of TI=(((*wall* AND carbon* AND nanotub*) OR *WCNT* OR (*WNT* AND carbon*)) AND (MW OR microwave)) for CNT and TI=(carbon* AND nano* AND (MW OR microwave)) for CNM

The intense microwave absorption of carbon nanotubes has been studied, though the mechanisms remain unclear[47]. The literature, overall, indicates that dielectric heating is efficient due to the high dielectric constant of the material (~200-300 for CNTs[48,49])[50]. Note that "perfect" CNTs are ballistic conductors, meaning that resistance is quantized and independent of length and no energy is dissipated due to electron movement, such that microwave induced current is not converted to heat[50]; imperfections, such as doping and defects, permit the superheating behavior. Patton and Windle[45], however, argue that dipole rotation is not a loss mechanism, as any dipoles due to functionalization are arranged in such a manner that inhibit dipole rotation, and conclude that conduction losses are the dominant factor in energy absorption. SWCNTs and MWCNTs have similar rapid heating responses to microwave irradiation[51].

The heating behavior of CNTs have been exploited in various applications, as temperatures up to 2000 °C can be achieved with selective irradiation[52]. Morgan et al.'s incorporation of CNTs in epoxy produced a marked increase and prolongation in heating response in a rapid and uniform manner[53]. Sweeney et al. observe in carbon nanotube-polymer composites that a finite range of loading is suitable: a minimum quantity of MWCNTs is required to achieve a rapid heating response and at higher MWCNT loadings, the heating response decreases and becomes less uniform as the MWCNTs become more reflective to incident microwaves[54].

Microwave irradiation of CNTs can also produce other useful behaviors and transformations of the material. When exposed to microwave fields, CNTs also attenuate incident propagating waves, emit light, emit gas, and undergo intense mechanical motion[52,47]. Microwave irradiation is also frequently used in purification and modification of carbon nanotubes. MacKenzie et al.[55] report improved crystallinity of SWCNTs, as microwave energy

reorients sp^3 bonds into sp^2 hybridization. Preferential destruction of metallic nanotubes for semiconductor applications have also been proposed due to increased absorption efficiency of metallic CNTs[56,57]. Microwave-assisted functionalization, additionally, limits shortening and damage of CNTs by reducing reflux time and enhances loading[50].

2.5 Environment, Health, & Safety Implications

Carbon nanotubes have been likened to asbestos in terms of impact on the human respiratory system. Due to their size and shape characteristics (length, width, shape, and density), CNTs are readily inhaled. They may be cleared from the lungs through mechanisms as follows: mucociliary escalator (mucous traps foreign material, which is swallowed and expelled from the body), phagocytosis by alveolar macrophages, acidic dissolution, or translocation through alveolar wall and lung interstitium to lymphatic system[58]. Carbon nanotubes that persist in the lungs may stimulate alveolar macrophages and epithelial cells, which will attract leukocytes[4]. The activity of these leukocytes can damage the alveolar wall, induce cellular and DNA damage, and stimulate proliferation of lung fibroblasts. This can result in conditions including severe lung fibrosis, scarring, and lung cancer, that are similar to those caused by asbestos.

Carbon nanotubes, further, can act beyond the respiratory system. Cells may incorporate CNTs through endocytosis or phagocytosis, which are both energy-dependent processes that are hindered at low temperatures and low ATP concentration[59]. While short CNTs can be readily incorporated into the cytosol, longer CNTs may float freely in the lymphatic system or blood stream, spreading inflammation. Through nanopenetration, functionalized nanotubes may diffuse across cellular membranes in an energy-independent process[4,59]. Such incorporations can cause toxicity through activation of multiple pathways, many damaging to DNA[59]. The CNTs can be carcinogenic, causing free radical generation, physical interference with mitosis, stimulation of

target cell proliferation, and/or persistent chronic inflammation[58]. Accumulation of CNTs can occur in the body, with biodistribution concentrated in the liver, spleen, lungs, and excretory system, largely due to CNTs trapped in capillaries[59]; bioaccumulation can be measured by near-infrared fluorescence (for only unbundled SWCNTs), chemothermal oxidation, and TGA in environmental applications[60].

Studies on toxicity demonstrate widespread inconsistency, with toxicity concentration ranges spanning six orders of magnitude[59]. This can likely be attributed to variation in characteristics of the nanotubes and lack of response comparison between cell types in each study. Additionally, contamination due to the synthesis process can affect the responses; various functional groups can be biocompatible or toxic. Health and safety analysis is further complicated by synthesis product inconsistency through variation in local and/or overall charge, catalyst residue, and length.

In their production and/or use, CNTs may be released into the environment, where they can interact with aquatic surfaces and biological species. Aggregation behavior provides insight into the fate and transport of CNTs. Aggregation allows the suspended CNTs to sediment and fall out of solution, limiting their impact on the environment; however, dispersion reduces potentially toxic concentrated nanomaterial deposition. Saleh et al.[61] observe that MWCNTs can form stable suspensions in conditions emulating typical aquatic environments; however, increased salt concentrations, decreased pH, and decreased natural organic matter increase the rate of aggregation as per the Derjaguin-Landau-Verway-Overbeek (DLVO) and non-DLVO steric interactions. Sano et al.[62] demonstrate that this holds for a variety of ionic salts, and offer that functionalization, in which ultrasonication in strong acids cut CNTs, allows for stable

dispersion of SWCNTs. Solubility enhancement can further be pursued with surfactants[63,64] or adsorbed polymers[65].

Section 3: CNT Functionalization and Characterization

3.1 Introduction

To improve MWCNT dispersion in the device, MWCNTs were functionalized prior to incorporation. Behavior of microwave irradiated fMWCNTs is not well studied; however, research by Vázquez and Prato[50] suggest that the presence of defects and dopants enable the superheating behavior. Functionalization additionally allows for enhancements in structural, electrical, and thermal properties.

3.2 Experimental

3.2.1 Materials

MWCNTs were obtained from Cheap Tubes, Inc. (Brattleboro, VA) with OD of 30-50 nm, length of 10-20 μm, and purity of >95 wt-%. Concentrated, reagent grade H_2SO_4 and HNO_3 were obtained from Fisher Scientific (Houston, TX). Synergy Ultrapure water and polytetrafluoroethylene (PTFE) membrane filters were obtained from EMD Millipore (Darmstadt, Germany).

3.2.2 Functionalization of MWCNTs[v]

1 g of MWCNTs was dispersed in 150 mL H_2SO_4 and 150 mL HNO3 for 30 minutes with bath sonication. The solution was refluxed at 80 °C for 1.5 hours or 3 hours for the low and high functionalization treatments, respectively. Upon completion of reflux, the solution was cooled with ultrapure water, and then filtered with vacuum separation with 0.22 μm PTFE membrane filters. The filtrate was washed with deionized water and filtered a minimum of 5 times to neutralize pH. After the final filtration, the filter and fMWCNTs were placed in a

[v] Procedure based upon work by Dipesh Das and Jaime Plazas-Tuttle

desiccator. Once dried, the fMWCNTs were powdered by hand with a mortar and pestle and stored in an air-tight container.

3.2.3 Characterization

A multiplicity of tools was used in order to observe the extent of functionalization and verify the experimental product. Pristine MWCNTs, Low fMWCNTs, and High fMWCNTs were compared in each characterization method.

Aggregation Behavior

An ALV/CGS-3 Precision Compact Goniometer System (ALV-Laser Vertriebsgesellschaft.m-b.H., Langen/Hessen, Germany) equipped with a 22 mW HeNe laser (equivalent to 800 mW at 532nm) was used to monitor aggregate average hydrodynamic radii through dynamic light scattering. Comparable concentrations of pristine MWCNTs, Low fMWCNTs, and High fMWCNTs were analyzed for 30 second intervals over 25 minutes.

A JEOL 2010F Transmission Electron Microscope at the Texas Materials Institute (JEOL USA Inc., Peabody, MA) was used to visually and qualitatively observe aggregation behavior of the samples, prepared from aqueous solutions of pristine MWCNTs, Low fMWCNTs, and High fMWCNTs.

Composition

X-ray photoelectron spectroscopy (XPS) was performed with a Kratos X-ray Photoelectron Spectrometer – Axis Ultra DLD (Kratos Analytical Ltd., Manchester, UK) at the Texas Materials Institute to determine elements and bond types. CasaXPS (Casa Software, Teignmouth, UK) was used for peak fitting.

Raman spectroscopy was performed with a WITec Micro-Raman Spectrometer alpha300

R at the Texas Materials Institute (WITec Instruments Corp., Knoxville, TN) and analyzed with WITec Project 2.08. The extent of defects was measured through peak shift and peak intensity analysis.

3.3 Results and Discussion

3.3.1 Dynamic Light Scattering

Suspensions of equal concentration for each of the three treatments were prepared with ultrapure water. Brief bath sonication mixed the suspensions. Analysis with dynamic light scattering indicate that pristine and functionalized MWCNTs display differing aggregation behavior, as seen in Figure 3.

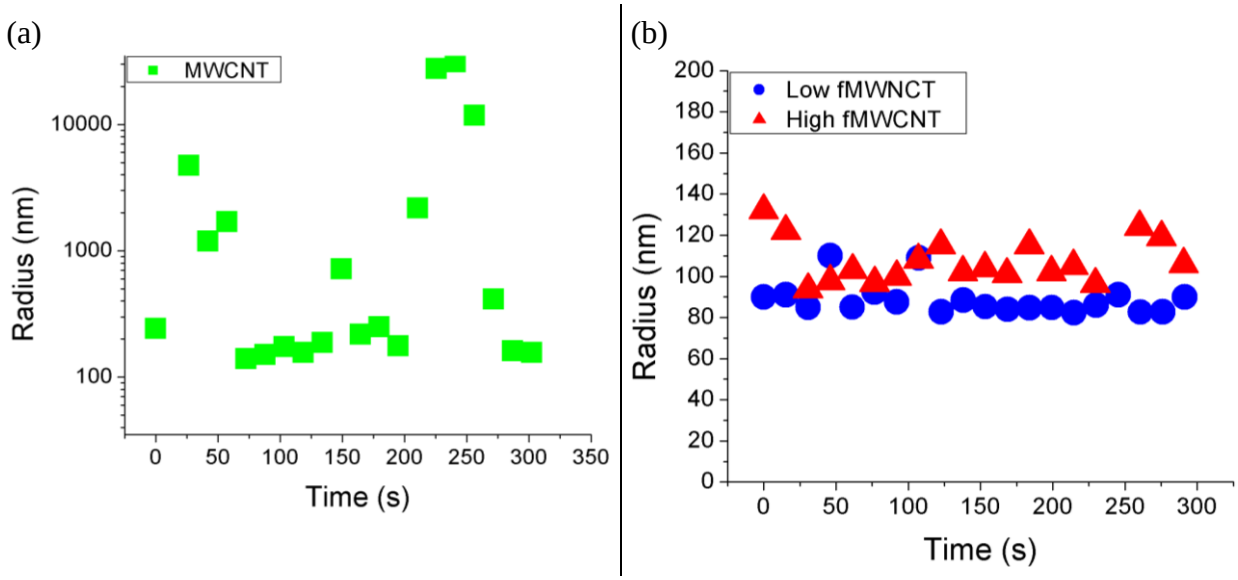

Figure 3: DLS of pristine and functionalized MWCNTs

Pristine MWCNTs exhibit aggregation, as the hydrodynamic radius ranged from 100 nm to over 10,000 nm. Nanomaterial aggregates were discernible by the human eye in the suspension. Although the measurements were not stable over time, there does not appear to be a pattern of aggregation behavior. The low solubility of Pristine MWCNTs is expected, as they

contain few or no sites for further ionic or covalent interaction, so van der Waals and steric interactions dominate the behavior of Pristine MWCNTs.

Both Low fMWCNTs and High fMWCNTs exhibited low aggregation, with average hydrodynamic radii of 88.7 nm and 107.5 nm, respectively. The radii are stable, exhibiting low variation over time with standard deviations of 7.77 nm for Low fMWCNTs and 10.71 nm for High fMWCNTs. Chemical functionalization alters the surface properties of the CNTs, such that they disperse readily in aqueous solutions. Longer reflux time corresponds to increased functionalization, which should result in lower radii. Although the radii are comparable, the data show the low functionalization treatment has lower hydrodynamic radii. This is likely due to incomplete neutralization of the acids used in functionalization, as the dissociated functional groups would interact more strongly with the polar water molecules. Subsequent characterization agrees with this assessment, showing that the Low fMWCNTs are less oxidized than the High fMWCNTs.

3.3.2 High Resolution Transmission Electron Microscopy

HRTEM was similarly used to visually demonstrate in Figure 4 the aggregation behavior of the Pristine MWCNTs, Low fMWCNTs, and High fMWCNTs. The Pristine MWCNTs exhibit significant aggregation, with regions of tangled carbon nanotubes. In contrast, both the Low fMWCNTs and High fMWCNTs are more uniformly distributed on the TEM grid, with low aggregation.

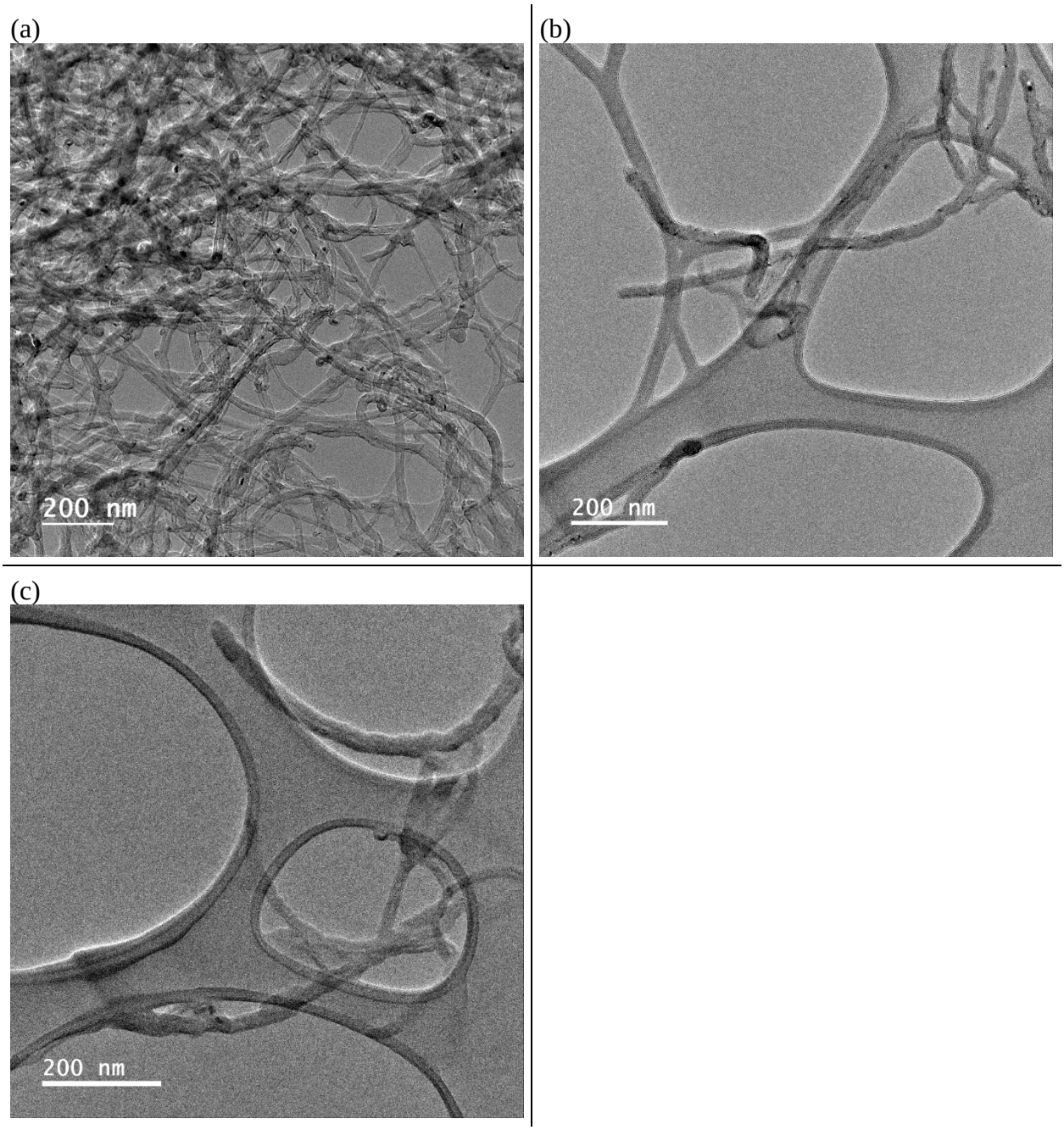

Figure 4: HRTEM of pristine and functionalized MWCNTs
The images correspond to (a) Pristine MWCNTs, (b) Low fMWCNTs, and (c) High fMWCNTs

3.3.3 Raman Spectroscopy

Raman spectroscopy in Figure 5 demonstrates the crystallinity of the carbon structures for each treatment. Each demonstrates the characteristic *D* mode (at ~1350 cm^{-1}) and the *G* mode (at ~1590 cm^{-1}). Notable peak characteristics are tabulated in Table 2; although many peaks are

identifiable, few are well studied, so this discussion will be limited to primarily the *D* and *G* modes.

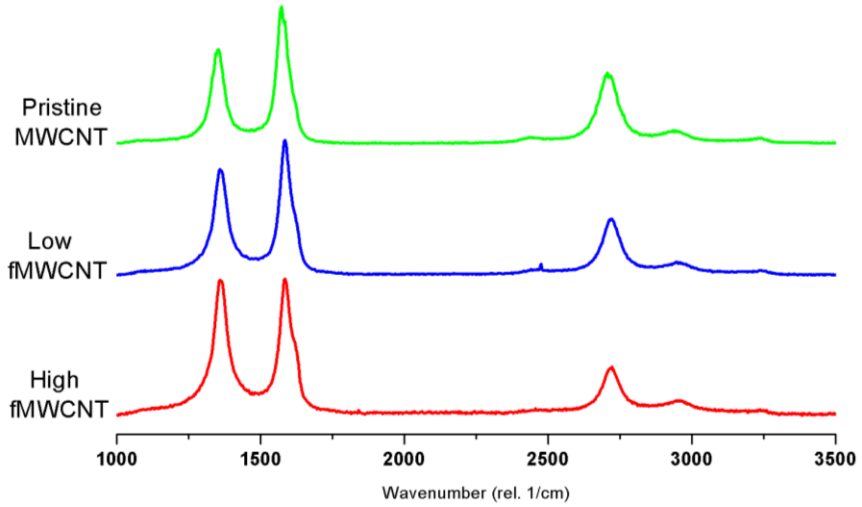

Figure 5: Raman spectroscopy of pristine and functionalized MWCNTs
Peak heights are normalized for equivalent *G* mode height across treatments.

Table 2: Raman spectroscopy peak locations for pristine and functionalized MWCNTs

Peak	Pristine MWCNT	Low fMWCNT	High fMWCNT
D	1354.66	1358.23	1358.23
G (E_{2g})	1571.2	1583.83	1583.83
	2430.75	2440.42	2456.54
*D** / *G'*	2703.33	2720.82	2720.82
D+*G*	2931.81	2946.58	2949.11
$2E_{2g}$	3232.42	3242.17	3232.41

In a comparison between Pristine MWCNTs and the functionalized treatments, each functionalized peak is upshifted. The oxidation process exerts pressure on the nanotubes, driving this upshift[39]. Note that in the *G* peak, a convoluted *D'* peak is more readily apparent with

increased functionalization; this peak is associated with the defect induced, double resonance process in Raman spectroscopy[39,41].

Extent of functionalization is quantitatively analyzed through the I_D / I_G ratios, tabulated in Table 3. Increased reflux time corresponds to increased I_D / I_G ratios, as amorphous disordered carbon, covalent modification, and defects increase the height of the *D* mode[4,39]. The *D* mode in the Pristine MWCNTs may arise due to nanotube cutting in sonication and impurities and/or defects in manufacture. The height of the *D* mode of Low fMWCNTs and High fMWCNTs are higher, signifying functionalization and defect creation. As the I_D / I_G ratio for the High fMWCNTs is higher, it can be concluded that the High fMWCNTs have more structural defects or modification than the Low fMWCNTs.

Table 3: Raman I_D / I_G ratios for pristine and functionalized MWCNTs

MWCNT Type	I_D / I_G
Pristine MWCNT	0.679
Low fMWCNT	0.783
High fMWCNT	0.991

Intensities in calculation correspond to peak maxima.

3.3.4 X-Ray Photoelectron Spectroscopy

XPS permits bond type identification for the three MWCNT treatments. In the three sets of XPS results, displayed in Figure 6, three prominent peaks were identified: O KLL Auger emission, O 1s emission, and C 1s emission. As the Auger emission is a secondary emission process, arising from a coincidence of ejected and filling electrons, it will be disregarded in the subsequent analysis.

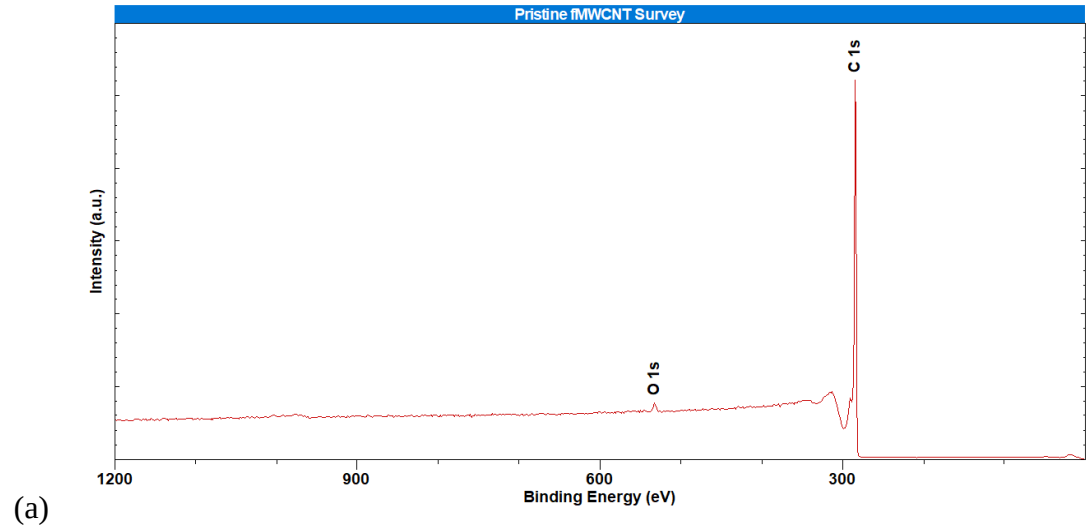

(a)

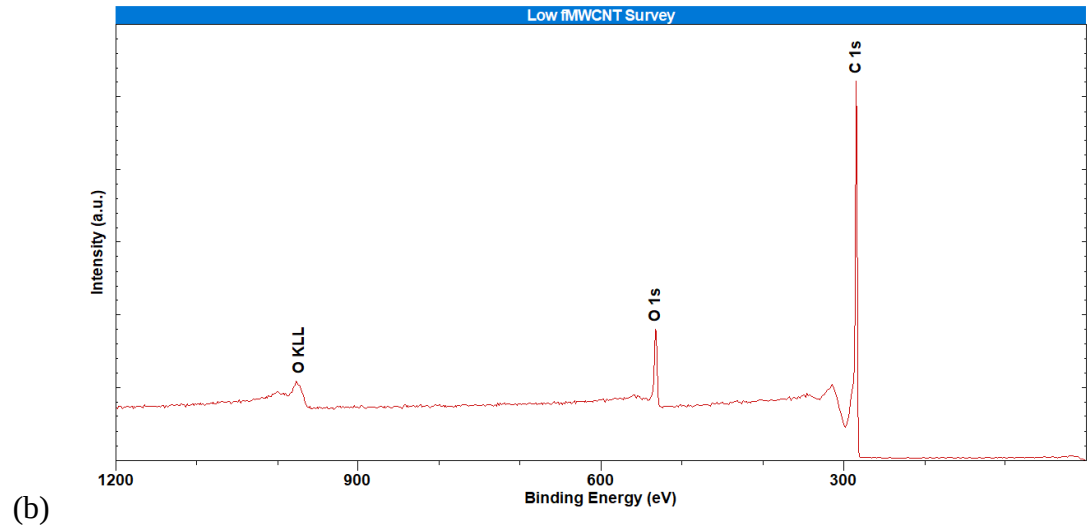

(b)

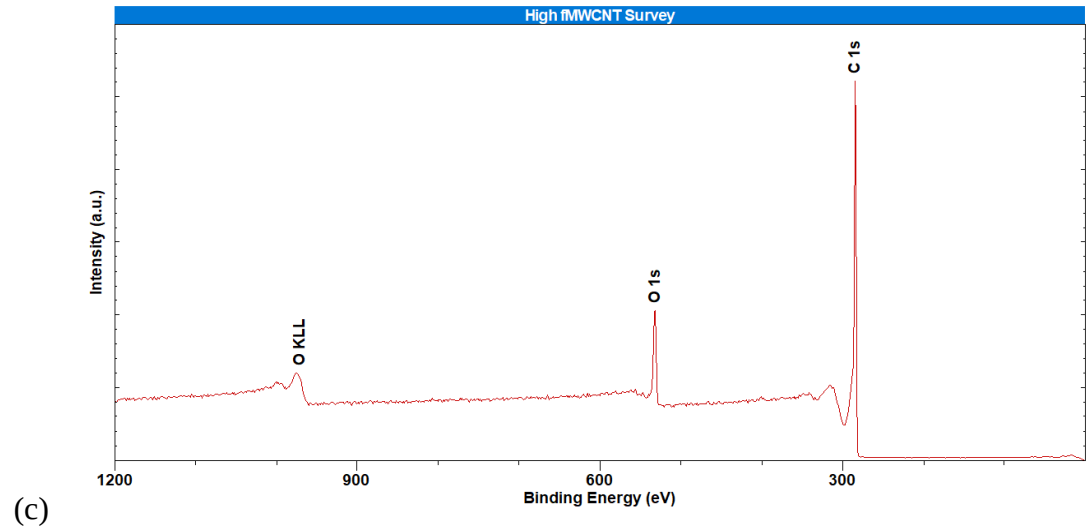

(c)

Figure 6: Survey XPS of pristine and functionalized MWCNTs
(a) corresponds to Pristine MWCNTs, (b) to Low fMWCNTs, and (c) to High fMWCNTs.

Through comparison of areas for the O 1s and C 1s peaks, the elemental composition of the MWCNT types are determined and displayed in Table 4. With increased functionalization, oxygen content increases, as anticipated.

Table 4: Peak summary for survey XPS of pristine and functionalized MWCNTs

MWCNT Type	Peak	Position (eV)	FWHM (eV)	Atomic %
Pristine MWCNTs	O 1s	533.10	3.70	0.89
	C 1s	285.10	2.33	99.11
Low fMWCNTs	O 1s	533.10	3.75	7.75
	C 1s	285.10	2.41	92.25
High fMWCNTs	O 1s	532.10	3.78	9.13
	C 1s	285.10	2.40	90.87

Peak analysis allows determination of bond types in the material. Figure 7 displays C 1s and O 1s peak deconvolution for each MWCNT type. Note the O 1s peak for Pristine MWCNTs is not well formed, as oxygen concentration is less than 1% overall and has poor signal as a result. In each O 1s peak observation, both O-C and O=C bonds are present with approximately equal O-C and O=C concentrations (Table 5).

Table 5: Peak summary for O 1s XPS of pristine and functionalized MWCNTs

MWCNT Type	Peak	Position (eV)	FWHM (eV)	Atomic %
Pristine MWCNTs	O-C	533.17	2.06	43.83
	O=C	531.47	2.31	56.17
Low fMWCNTs	O-C	533.38	1.83	45.17
	O=C	531.77	1.97	54.83
High fMWCNTs	O-C	533.40	1.92	47.23
	O=C	531.71	1.91	52.77

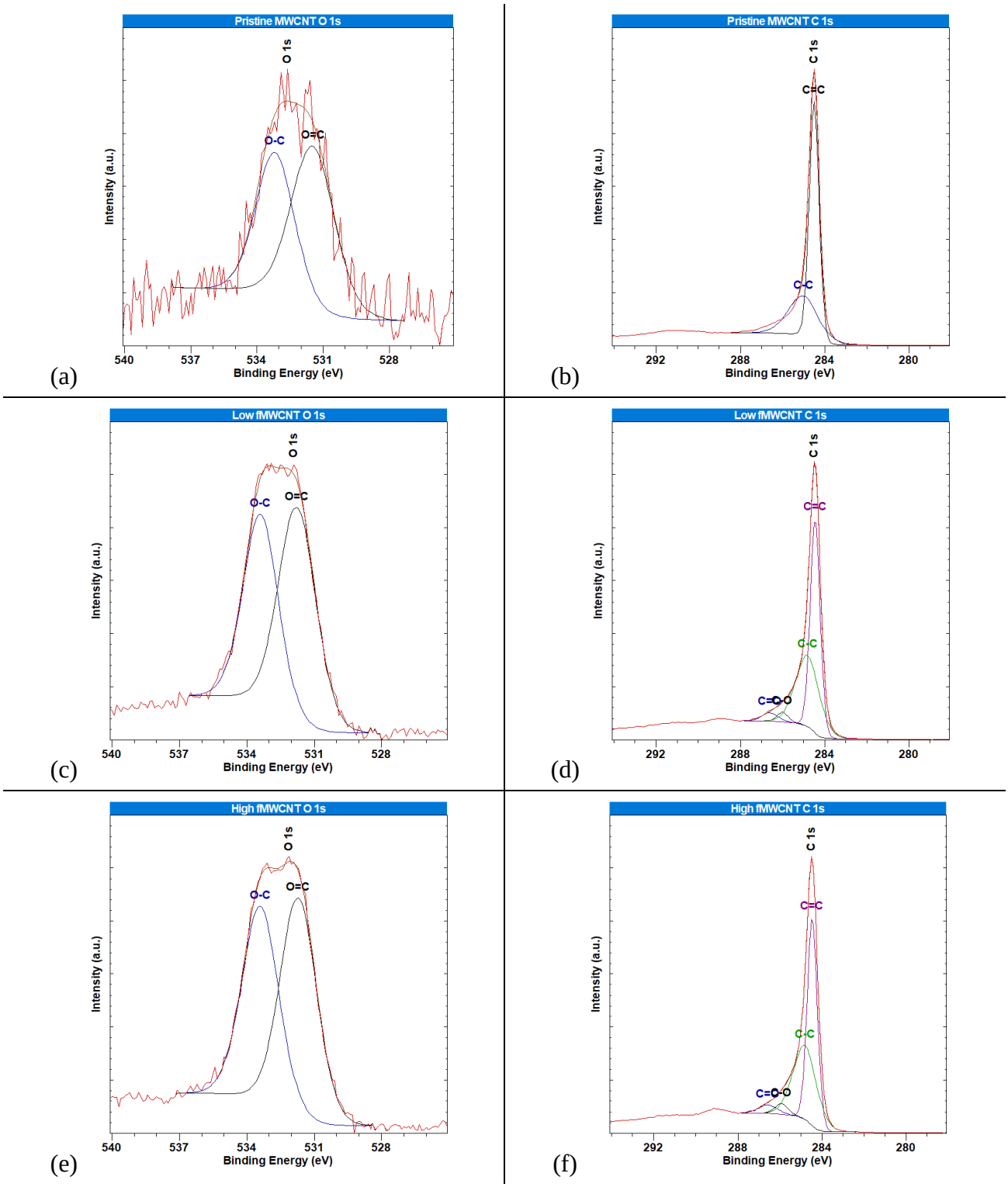

Figure 7: Peak deconvolution of XPS of Pristine and functionalized MWCNTs (a) and (b) correspond to pristine MWCNTs, (c) and (d) to Low fMWCNTs, and (e) and (f) to High fMWCNTs. (a), (c), and (e) display deconvolution of the O 1s peaks and (b), (d), and (f) of C 1s peaks.

Deconvolution of the C 1s peaks (Table 6) enables a determination of the defects and functionalization of the nanotubes. Comparing the Low and High fMWCNTs against the Pristine MWCNTs, some of the stable C=C bonds have broken, with a majority resulting in C-C bonds. Nonnegligible quantities of C-O and C=O bonds also arise; note the ratio between O-C and O=C bonds from the deconvolution of the O 1s peak were retained for the deconvolution of the C 1s peak. Between Low and High fMWCNTs, High fMWCNTs have higher atomic percentages of C-C, C-O, and C=O bonds, though are close in value. Oxygen content via peak analysis of the C 1s peak is lower than that in the overall XPS peaks, suggesting additional oxygen bonding in forms such as COO and O-COO that were not analyzed and/or other oxygen-containing contamination.

Table 6: Peak summary for C 1s XPS of pristine and functionalized MWCNTs

MWCNT Type	Peak	Position (eV)	FWHM (eV)	Atomic %
Pristine MWCNTs	C-C	284.98	1.71	33.69
	C=C	284.5	0.55	66.31
Low fMWCNTs	C-C	284.81	1.30	41.40
	C=C	284.45	0.55	52.72
	C-O	285.99	0.62	2.66
	C=O	286.59	0.84	3.23
High fMWCNTs	C-C	284.81	1.30	41.87
	C=C	284.46	0.56	51.06
	C-O	285.91	0.75	3.34
	C=O	286.56	1.05	3.73

Section 4: Device Development and Microwave Irradiation

4.1 Introduction

In this study, MWCNTs and fMWCNTs are to be immobilized in a disk to measure heating induced by the thermal conductivity of carbon nanotubes. In previous work[66] by Rowles, silver nanoparticles were affixed in a glaze to ceramic disks in order to release ionic silver for antibacterial action. For this study, it was desired that CNTs be incorporated into the disk in lieu of coating the disk; consequently, Rowles' ceramic disk method could not be adapted for use, as the ceramic disks were fired at 1100 °C, while MWCNTs decompose[67,68] between 400 °C and 500 °C.

For a lower temperature-firing matrix, plaster of Paris was used. Cement was added to reduce the solubility of plaster of Paris, as the device was to be used in water. Sugar was used as a pore-forming material, as it decomposes at 185.5 °C. With these materials, the disks could be fired at 225 °C to decompose off the pore-forming material yet prevent the decomposition of the MWCNTs. A wetting and drying step was added to enable the cement to bind the components.

4.2 Experimental

4.2.1 Materials

Pristine MWCNTs were obtained from Cheap Tubes Inc. (Brattleboro, VT) and two treatments of fMWCNTs were synthesized from the same with 1.5-hour and 3.0-hour reflux times. Plaster of Paris and Portland cement were from laboratory stock. Turbinado sugar was obtained from Sugar In the Raw® (Brooklyn, NY) and ground before use. Synergy Ultrapure water was obtained from EMD Millipore (Darmstadt, Germany).

For cartridge preparation, two ½" low-carbon steel rods (McMaster-Carr) were used in conjunction with ½" ID PVC to form a die. The hydraulic press used was an L-16 16-ton press

manufactured by Research & Industrial Instruments Company (England, United Kingdom). For firing, a Thermo Scientific Lindberg Blue M tube furnace (Waltham, MA) was used.

To determine microwave heating, a conventional 1.4 cu. ft. countertop microwave oven (Model JES1460DS2BB) with the internal lamp removed was used, manufactured by GE® (Rapid City, SD). Temperature measurement was completed with an OMEGA™ Digital Handheld Temperature Calibrator (Model CL3512A) with a K-type thermocouple manufactured by OMEGA Engineering, Inc. (Norwalk, CT).

4.2.2 Device Preparation

A four-step process was used to produce testable MWCNT-containing cartridges; see Figure 8 for a simplified visual of the process. First: 300 mg mixtures for each cartridge were made, with 1%, 2%, and 5% compositions of MWCNT of interest described in Table 7 for pristine MWCNTs, 1.5-hour reflux fMWCNTs, and 3.0-hour reflux fMWCNTs. Blanks were additionally produced, and all cartridges were made in triplicate. Second: each recipe was mixed by hand until uniform in appearance and dry-pressed into a ½" diameter coupon. (A wet method was attempted, however was discarded as disk separation from the mold proved challenging.) A hydraulic press applied 10 tons of pressure on ram on the materials in the die for 30 seconds. Third: approximately 20 μL of ultrapure water was deposited on each face of the compacted cartridges and the cartridges allowed to air-dry for 24 hours. Fourth: cartridges were subsequently heated to 225 °C in a tube furnace at a temperature ramp of 1 °C/min. The cartridges were held at 85 °C for one hour below the boiling point of water before continuing the temperature ramp and held at the max temperature for one hour prior to slow cooling at 1 °C/min.

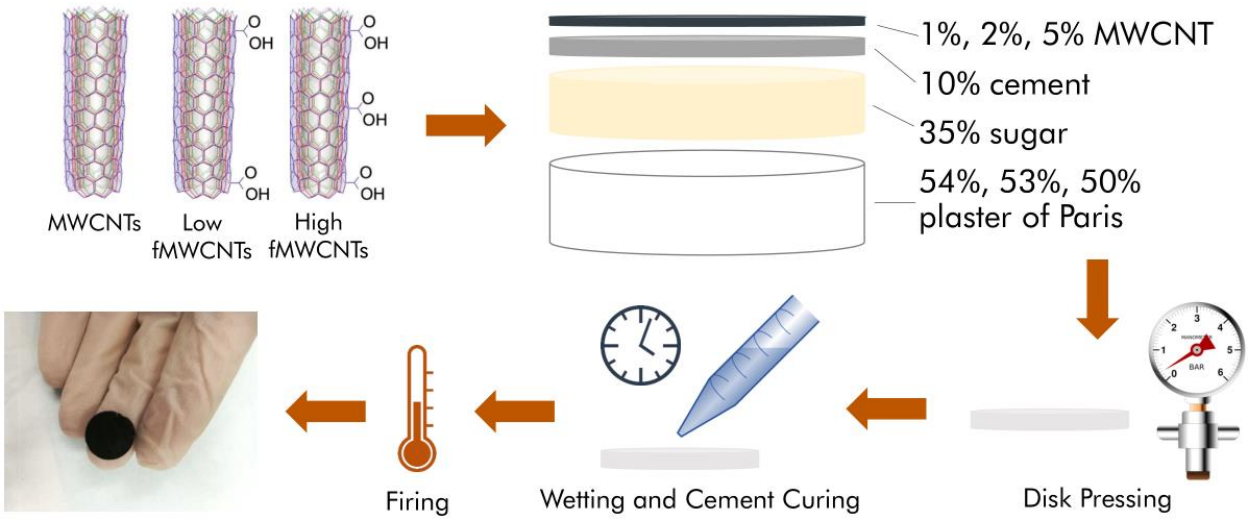

Figure 8: Simplified nano-enabled disk preparation graphic

Table 7: Composition of nano-enabled disks

Component	Weight* (mg)			
	1%	2%	5%	Blank
MWCNT	3	6	15	--
Cement	30	30	30	30
Sugar	105	105	105	--**
Plaster of Paris	162	159	150	165
Total	300	300	300	300

* MWCNTs ±0.10 mg; all other measurements ±0.50 mg
** Sugar was omitted from the blanks as it produced poorly formed, untestable blanks

4.2.3 Design of Experiment

To determine pore volume, thickness and diameter of each disk was measured in three locations. Each disk was weighed, boiled in excess ultrapure water for 1 hour, allowed to saturate for 24 hours, and reweighed. The difference between the saturated and dry masses provided the mass of water contained in the disks, and consequently, the porosity.

Each disk was placed in a vial with ultrapure water to total to 1 mL water. Initial temperature was measured and recorded, before microwaving the capped vial for a specified time interval. The microwave was operated at 10% power for time intervals up to 3.5 minutes, with 30 second increments between selected measurements. Final temperature was recorded, and the vial placed in an ice bath to cool to approximately room temperature before the experiment was repeated for the disk at all microwave time intervals of interest. Disks that dissolved were replaced by comparable disks.

4.3 Results and Discussion

4.3.1 Observations

30 disks were prepared for the experiment, in order to collect data in triplicate, shown in Figure 9. Disks poorly formed or broken upon removal from tube firing were replaced, as well as disks that dissolved in the saturation step. Such failures may have arisen due to uneven distribution of components; for example, concentration of sugar may have caused bubbling in the tube firing. Note that tested disks were not entirely uniform in shape, some bubbling, cracks, and chips were present.

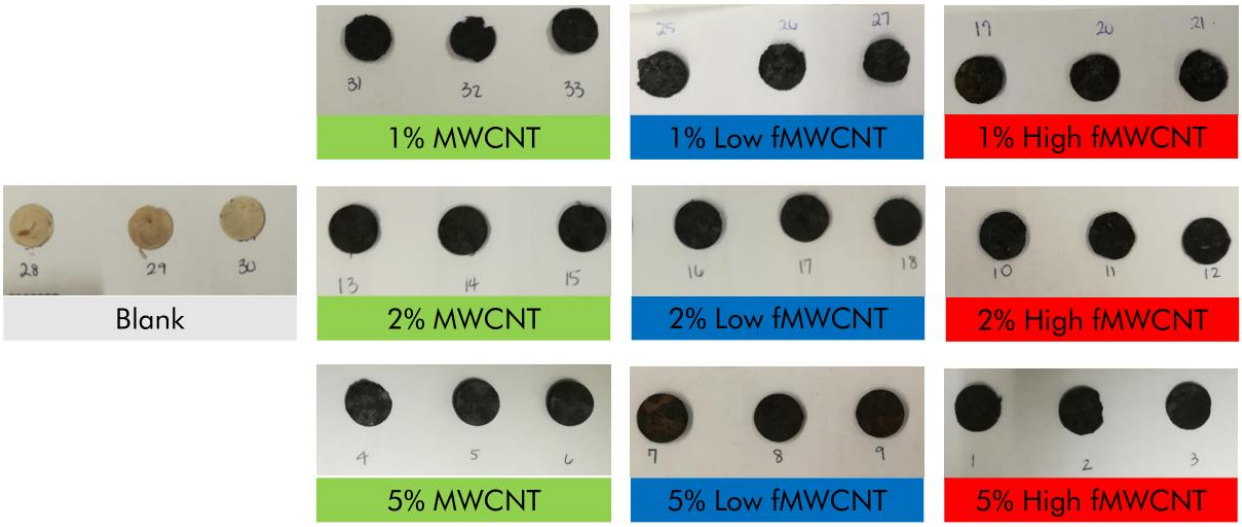

Figure 9: Nano-enabled disks in triplicate

4.3.2 Porosity

Porosity of each disk containing MWCNTs varied from 27% to 65%; averages of each disk type are presented in Table 8, with an overall average of 41% porosity. Each disk was composed of 35% ground sugar, so the calculated averages are as expected. The average porosity of the blanks (containing no pore-forming agent) was 8%, allowing that a limited fraction of the porosity is due to factors beyond the addition of ground sugar as a pore-forming agent. The size of the ground sugar granules was not measured, and observations of each disk type are few, so observations of seeming trends of porosity should not be concluded from this data.

Table 8: Porosity of nano-enabled disks

MWCNT Type	**MWCNT Amount**			
	1%	**2%**	**5%**	**Average**
Pristine MWCNT	40%	38%	53%	44%
Low fMWCNT	33%	45%	45%	41%
High fMWCNT	32%	37%	43%	37%
Average	35%	40%	47%	41%

Each data porosity value is an average of computed porosity for 3 similar disks
Note 1% High fMWCNT is calculated from data of only 2 disks.

4.3.3 Microwave Heating

Microwave heating was compared at each loading of MWCNTs for blanks, Pristine MWCNTs, Low fMWCNTs, and High fMWCNTs in Figure 10.

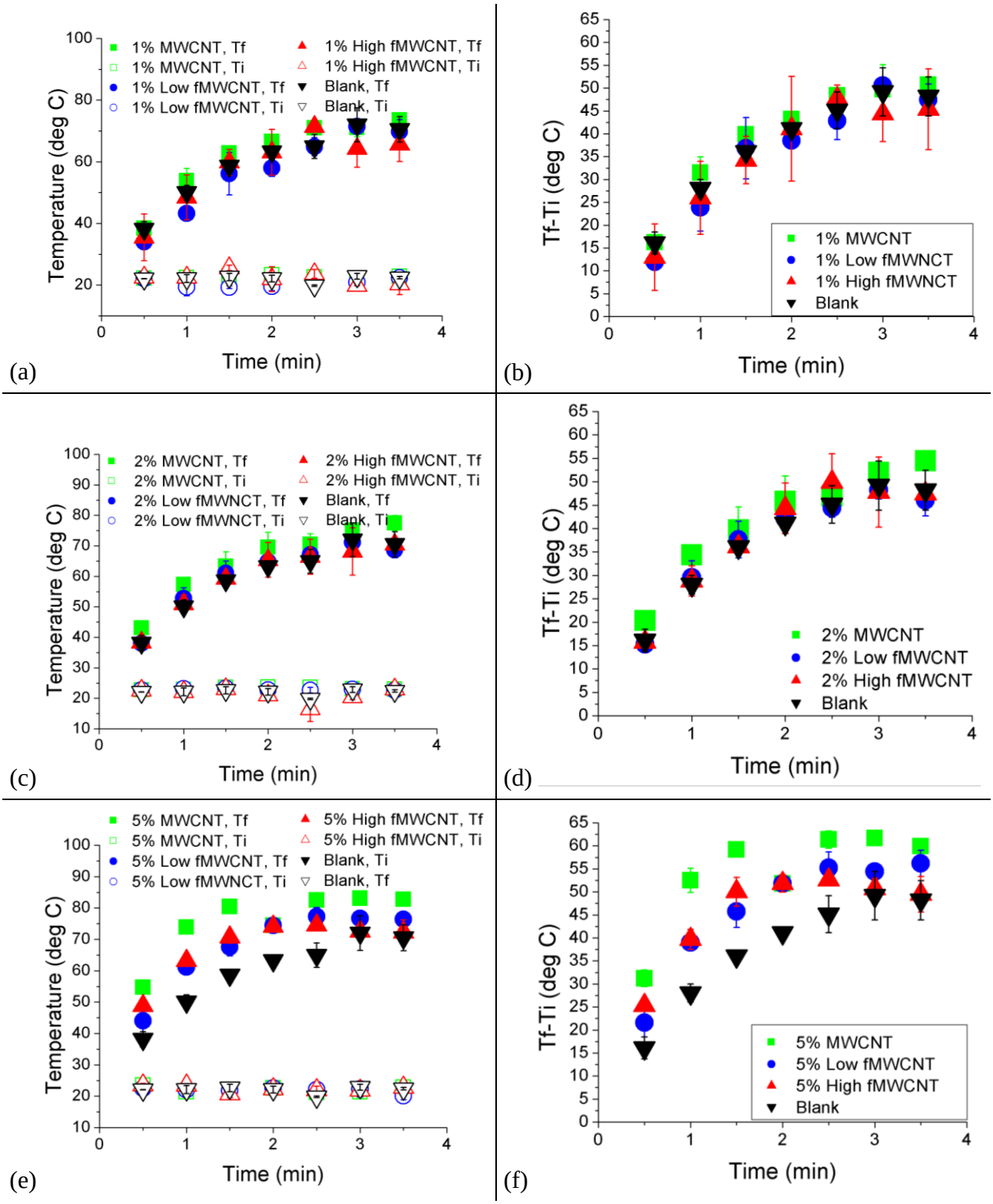

Figure 10: Microwave-induced temperature change on nano-enabled disks
(a), (c), and (e) demonstrate the average of 3 initial and final recorded water temperatures for each disk type. (b), (d), and (f) demonstrate the average of 3 recordings of the change in water temperature for each disk type.

At low MWCNT loadings, temperature difference upon microwave irradiation is largely consistent across each of the test conditions. At 1% and 2% loadings, Pristine MWCNTs often exhibit higher temperature change than the other treatments; however, the overlapping confidence intervals suggest that this difference may result from random variation. Such similarity is expected, and consistent with Sweeney et al.'s findings of a minimum required loading[54].

At 5% loading, a clear difference in heating behavior can be seen. Compared to the blanks, the Pristine MWCNTs, Low fMWCNTs, and High fMWCNTs display increased heating. The Low fMWCNTs and High fMWCNTs display comparable results, while Pristine MWCNTs demonstrate further heating with statistical significance. After one minute of microwave irradiation, the MWCNT treatments exhibit additional temperature increases of approximately 25 °C and 10 °C for Pristine MWCNTs and both Low and High fMWCNTs, respectively, compared against the blanks.

The heating behavior with MWCNTs is initially rapid, however, begins to plateau at higher microwave times. This behavior suggests a saturation of MWCNT heating ability. Experimentation with greater loading of the MWCNT treatments can verify this hypothesis. Nonetheless, the MWCNTs appear to plateau at higher temperatures than the blanks, such that the microwave irradiation treatment produces both rapid and enhanced heating abilities.

Section 5: Conclusions and Recommendations

In this thesis, the design and synthesis of a nano-enabled device that can harness the power of microwave irradiation towards water treatment applications was studied. The results show promise; however, further study is necessary before implementation of the technology.

OBJECTIVE 1. Perform a literature review to understand the properties of carbon nanotubes and derivative materials.

A review was performed to provide foundational knowledge of carbon nanotubes, modification, effects of microwave irradiation, and environmental, health, and safety concerns. During this review, it was found that microwave irradiation of carbon nanotubes is a field of growing study. Current implementations attest that CNT incorporation allows for rapid, uniform heating of materials, making them a promising material for enhanced heating behavior towards bacterial inactivation. However, the corpus of knowledge remains small for such an application of CNTs, presenting many opportunities for optimization.

OBJECTIVE 2. Develop a PP matrix to immobilize carbon nanotubes.

To contain the MWCNTs, a plaster of Paris matrix was developed. A base of plaster of Paris and Portland cement provided structural integrity in an aqueous environment, and sugar permitted formation of pores for increased permeability and CNT contact area. Ratios were determined such that the device would be well-formed and retain its shape. No visible leeching into water was observed from the devices; however, microscopy, nuclear magnetic resonance (NMR), and/or Raman spectroscopy could assist in determination of CNTs or metal ions in solution.

OBJECTIVE 3. Vary degree of heating caused by devices.

Microwave irradiation experiments with multi-wall carbon nanotube treatments in plaster of Paris matrices demonstrate improved heating behavior with the incorporation of MWCNTs. Both bare and functionalized MWCNTs can improve interfacial heating; however, a minimum level of MWCNTs is required to observe an effect. Statistically significant differences in heating were observed at a loading of 5% MWCNTs for all treatments. A trade-off exists between increased heating and increased dispersion (or extent of oxidation) of MWCNTs. Such results suggest that increased defects and oxygen concentration can have an inverse effect on the heating behavior of MWCNTs. Nonetheless, at higher microwave irradiation times, the MWCNTs appear to have been saturated and their heating behavior leveled off, with values for the Pristine MWCNTs, Low fMWCNTs, and High fMWCNTs seeming to converge.

FUTURE WORK

Though this thesis provides an initial approach into product development, further study is necessary before testing and commercialization is possible. The increased heating achieved by the combination of carbon nanotubes and microwave irradiation has not been assessed for effectiveness in bacterial inactivation. Optimization of the PP matrix, additionally, has not been completed. Furthermore, analysis of the device behavior upon scaling to larger quantities of water remains.

Future work can focus on the following key areas:

- Incorporation of hybrid CNTs, such as Ag NP hybrids, to harness additional bactericidal mechanisms
- Investigation of dispersion of CNTs in device
- Development of a wet-press device preparation method to increase dispersion of fCNTs

- Identification of optimal CNT loading and microwave time to maximize heating
- Determination of CNT immobilization of device
- Optimization of device composition with regards to cost and structural integrity
- Assessment of device bacterial inactivation against common pathogens, including *E. coli*
- Scaling device design and use for realistic water consumption needs
- Development of a flow-through device allowing continuous water treatment
- Incorporation of such a flow-through device into a comprehensive domestic water treatment system capable of removing sediment, metal ions, and other contaminants
- Assessment of device safety and longevity
- Cost analysis of potential devices to assess affordability

Appendices

APPENDIX A: MICROWAVE HEATING EXPERIMENT

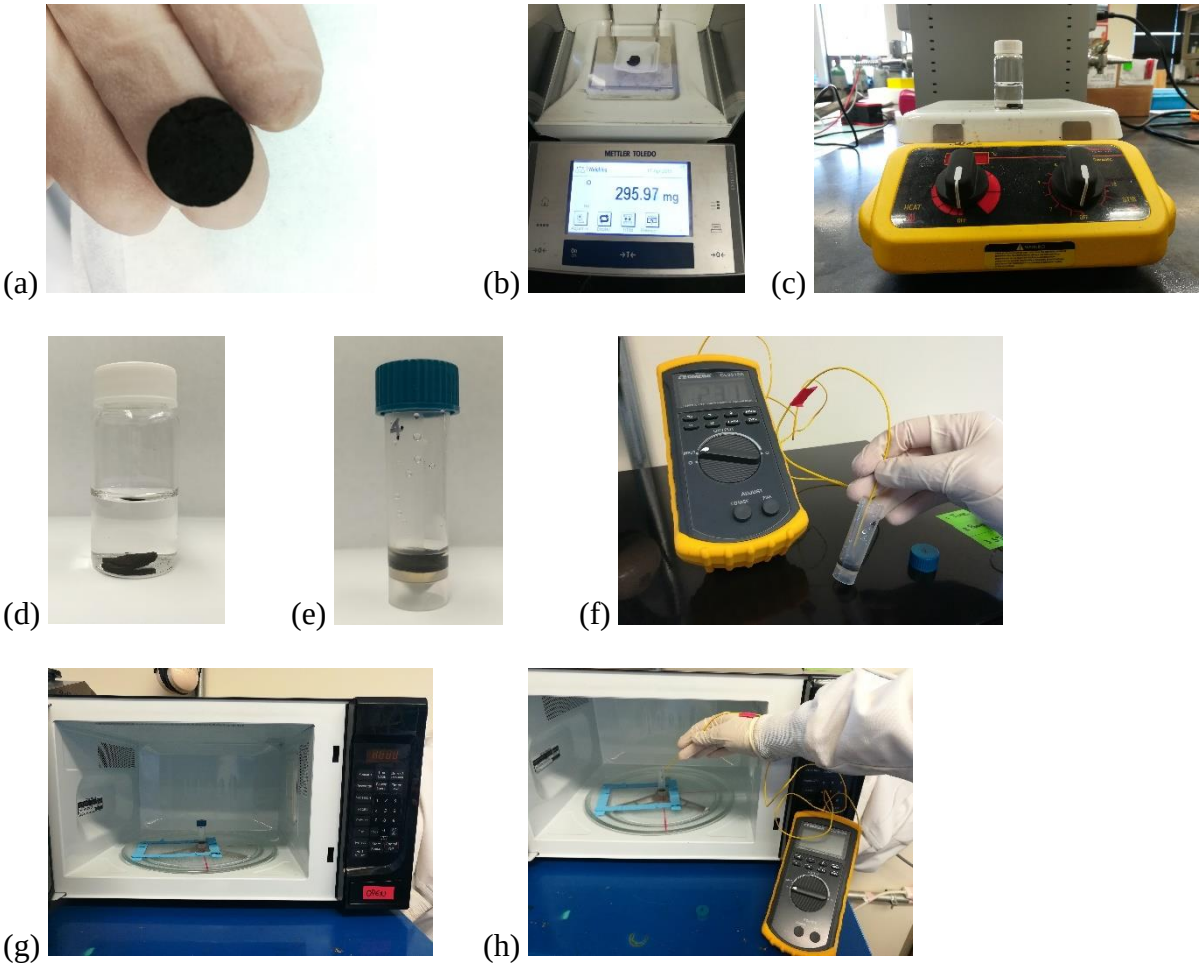

Figure 11: Microwave heating experiment setup
Physical characteristics of the MWCNT devices in (a) were collected, including weight (b) and size parameters. Each device was boiled (c) in excess Millipore water and allowed to saturate 24 hours (d). The device with Millipore water to total 1 mL was transferred into a vial (e) for the eating experiments. Initial temperature was recorded (f), and the loosely-capped vial microwaved (g) for a specified length of time. Immediately after microwaving, the cap was removed, and the temperature taken (h). The vial was recapped and placed in an ice bath until cooled to room temperature for repeat experiments.

References

(1) Allaire, M., Wu, H., & Lall, U. (2018). National trends in drinking water quality violations. *Proceedings of the National Academy of Sciences*, *115*(9), 2078–2083. doi:10.1073/pnas.1719805115

(2) United States Census Bureau. (2011). *Extended Measures of Well-being: Living Conditions in the United States*, 2011 [Data set]. Retrieved from https://www.census.gov/content/census/en/data/tables/2011/demo/well-being/p70-136.html

(3) Kaushik, B. K., & Majumder, M. K. (2014). Carbon Nanotube: Properties and Applications. *SpringerBriefs in Applied Sciences and Technology*, 17–37. doi:10.1007/978-81-322-2047-3_2

(4) Vajtai, R. (Ed.). (2013). *Springer Handbook of Nanomaterials*. doi:10.1007/978-3-642-20595-8

(5) Treacy, M. M. J., Ebbesen, T. W., Gibson, J. M. (1996). Exceptionally high Young's modulus observed for individual carbon nanotubes. *Nature*, *381*(6584), 678-680. doi: 10.1038/381678a0

(6) Yu, M. F., Lourie, O., Dyer, M. J., Moloni, K., Kelly, T. F., & Ruoff, R. S. (2000). Strength and Breaking Mechanism of Multiwalled Carbon Nanotubes Under Tensile Load. *Science*, *287*(5453), 637–640. doi:10.1126/science.287.5453.63

(7) Palaci, I., Fedrigo, S., Brune, H., Klinke, C., Chen, M., & Riedo, E. (2005). Radial Elasticity of Multiwalled Carbon Nanotubes. *Physical Review Letters*, *94*(17). doi:10.1103/physrevlett.94.175502

(8) Kis, A., Jensen, K., Aloni, S., Mickelson, W., & Zettl, A. (2006). Interlayer Forces and Ultralow Sliding Friction in Multiwalled Carbon Nanotubes. *Physical Review Letters*, *97*(2). doi:10.1103/physrevlett.97.025501

(9) Huhtala, M., Krasheninnikov, A. V., Aittoniemi, J., Stuart, S. J., Nordlund, K., & Kaski, K. (2004). Improved mechanical load transfer between shells of multiwalled carbon nanotubes. *Physical Review B*, *70*(4). doi:10.1103/physrevb.70.045404

(10) Locascio, M., Peng, B., Zapol, P., Zhu, Y., Li, S., Belytschko, T., & Espinosa, H. D. (2009). Tailoring the Load Carrying Capacity of MWCNTs Through Inter-shell Atomic Bridging. *Experimental Mechanics*, *49*(2), 169–182. doi:10.1007/s11340-008-9216-3

(11) Frank, S., Poncharal, P., Wang, Z. L., & de Heer, W. A. (1998). Carbon Nanotube Quantum Resistors. *Science*, *280*(5370), 1744–1746. doi:10.1126/science.280.5370.1744

(12) Bachtold, A., Strunk, C., Salvetat, J.-P., Bonard, J.-M., Forró, L., Nussbaumer, T., & Schönenberger, C. (1999). Aharonov–Bohm oscillations in carbon nanotubes. *Nature*, *397*(6721), 673–675. doi:10.1038/17755

(13) Schönenberger, C., Bachtold, A., Strunk, C., Salvetat, J.-P., & Forró, L. (1999). Interference and Interaction in multi-wall carbon nanotubes. *Applied Physics A: Materials Science & Processing*, *69*(3), 283–295. doi:10.1007/s003390051003

(14) Naeemi, A., & Meindl, J. D. (2006). Compact physical models for multiwall carbon-nanotube interconnects. *IEEE Electron Device Letters*, *27*(5), 338–340. doi:10.1109/led.2006.873765

(15) Li, H. J., Lu, W. G., Li, J. J., Bai, X. D., & Gu, C. Z. (2005). Multichannel Ballistic Transport in Multiwall Carbon Nanotubes. *Physical Review Letters*, *95*(8). doi:10.1103/physrevlett.95.086601

(16) Mattia, D., Rossi, M. P., Kim, B. M., Korneva, G., Bau, H. H., & Gogotsi, Y. (2006). Effect of Graphitization on the Wettability and Electrical Conductivity of CVD-Carbon Nanotubes and Films. *The Journal of Physical Chemistry B*, *110*(20), 9850–9855. doi:10.1021/jp061138s

(17) Kaneto, K., Tsuruta, M., Sakai, G., Cho, W. Y., & Ando, Y. (1999). Electrical conductivities of multi-wall carbon nano tubes. *Synthetic Metals*, *103*(1-3), 2543–2546. doi:10.1016/s0379-6779(98)00221-5

(18) Milne, W. I., Teo, K. B. K., Chhowalla, M., Amaratunga, G. A. J., Lee, S. B., Hasko, D. G., … Thien Binh, V. (2003). Electrical and field emission investigation of individual carbon nanotubes from plasma enhanced chemical vapour deposition. *Diamond and Related Materials*, *12*(3-7), 422–428. doi:10.1016/s0925-9635(02)00292-3

(19) Begtrup, G. E., Ray, K. G., Kessler, B. M., Yuzvinsky, T. D., Garcia, H., & Zettl, A. (2007). Probing Nanoscale Solids at Thermal Extremes. *Physical Review Letters*, *99*(15). doi:10.1103/physrevlett.99.155901

(20) Dragomana, M., Hartnagel, H. L., Tuovinen, J., & Plana, R. (2005). Microwave applications of carbon nanotubes. *Frequenz*, *59*(11-12). doi:10.1515/freq.2005.59.11-12.251

(21) Yang, D. J., Wang, S. G., Zhang, Q., Sellin, P. J., & Chen, G. (2004). Thermal and electrical transport in multi-walled carbon nanotubes. *Physics Letters A*, *329*(3), 207–213. doi:10.1016/j.physleta.2004.05.070

(22) Gaillard, M., Mbitsi, H., Petit, A., Amin-Chalhoub, E., Boulmer-Leborgne, C., Semmar, N., … Kouassi, S. (2011). Electrical and thermal characterization of carbon nanotube films. *Journal of Vacuum Science & Technology B, Nanotechnology and*

Microelectronics: Materials, Processing, Measurement, and Phenomena, *29*(4), 041805. doi:10.1116/1.3607317

(23) Choi, T. Y., Poulikakos, D., Tharian, J., & Sennhauser, U. (2005). Measurement of thermal conductivity of individual multiwalled carbon nanotubes by the 3-ω method. *Applied Physics Letters*, *87*(1), 013108. doi:10.1063/1.1957118

(24) Kim, P., Shi, L., Majumdar, A., & McEuen, P. L. (2001). Thermal Transport Measurements of Individual Multiwalled Nanotubes. *Physical Review Letters*, *87*(21). doi:10.1103/physrevlett.87.215502

(25) Yan, X. H., Xiao, Y., & Li, Z. M. (2006). Effects of intertube coupling and tube chirality on thermal transport of carbon nanotubes. *Journal of Applied Physics*, *99*(12), 124305. doi:10.1063/1.2206851

(26) Assael, M. J., Chen, C.-F., Metaxa, I., & Wakeham, W. A. (2004). Thermal Conductivity of Suspensions of Carbon Nanotubes in Water. *International Journal of Thermophysics*, *25*(4), 971–985. doi:10.1023/b:ijot.0000038494.22494.04

(27) Takahashi, H., Numao, S., Bandow, S., & Iijima, S. (2006). AFM imaging of wrapped multiwall carbon nanotube in DNA. *Chemical Physics Letters*, *418*(4-6), 535–539. doi:10.1016/j.cplett.2005.10.150

(28) Sanz, V., Borowiak, E., Lukanov, P., Galibert, A. M., Flahaut, E., Coley, H. M., … McFadden, J. (2011). Optimising DNA binding to carbon nanotubes by non-covalent methods. *Carbon*, *49*(5), 1775–1781. doi:10.1016/j.carbon.2010.12.064

(29) Du, J., Ge, C., Liu, Y., Bai, R., Li, D., Yang, Y., … Chen, C. (2011). The Interaction of Serum Proteins with Carbon Nanotubes Depend on the Physicochemical Properties of

Nanotubes. *Journal of Nanoscience and Nanotechnology*, *11*(11), 10102–10110. doi:10.1166/jnn.2011.4976

(30) Zhao, H., & Ju, H. (2006). Multilayer membranes for glucose biosensing via layer-by-layer assembly of multiwall carbon nanotubes and glucose oxidase. *Analytical Biochemistry*, *350*(1), 138–144. doi:10.1016/j.ab.2005.11.034

(31) Manesh, K. M., Kim, H. T., Santhosh, P., Gopalan, A. I., & Lee, K.-P. (2008). A novel glucose biosensor based on immobilization of glucose oxidase into multiwall carbon nanotubes–polyelectrolyte-loaded electrospun nanofibrous membrane. Biosensors and *Bioelectronics*, *23*(6), 771–779. doi:10.1016/j.bios.2007.08.016

(32) Zheng, D., Hu, C., Peng, Y., Yue, W., & Hu, S. (2008). Noncovalently functionalized water-soluble multiwall-nanotubes through azocarmine B and their application in nitric oxide sensor. *Electrochemistry Communications*, *10*(1), 90–94. doi:10.1016/j.elecom.2007.10.027

(33) Rakitin, A., Papadopoulos, C., & Xu, J. M. (2003). Carbon nanotube self-doping: Calculation of the hole carrier concentration. *Physical Review B*, *67*(3). doi:10.1103/physrevb.67.033411

(34) Thrower, P. A. (1969). Study of defects in graphite by transmission electron microscopy. *Chemistry & Physics of Carbon*, *5*, 217-319).

(35) Stone, A. J., & Wales, D. J. (1986). Theoretical studies of icosahedral C60 and some related species. *Chemical Physics Letters*, *128*(5-6), 501–503. doi:10.1016/0009-2614(86)80661-3

(36) Banerjee, S., Hemraj-Benny, T., & Wong, S. S. (2005). Covalent Surface Chemistry of Single-Walled Carbon Nanotubes. *Advanced Materials*, *17*(1), 17–29. doi:10.1002/adma.200401340

(37) Okpalugo, T. I. T., Papakonstantinou, P., Murphy, H., McLaughlin, J., & Brown, N. M. D. (2005). High resolution XPS characterization of chemical functionalised MWCNTs and SWCNTs. *Carbon*, *43*(1), 153–161. doi:10.1016/j.carbon.2004.08.033

(38) Casa Software, Ltd. (2013). Introduction to XPS with Examples of Spectra. *Manual Updates*. http://www.casaxps.com/help_manual/manual_updates/xps_spectra.pdf

(39) Murphy, H., Papakonstantinou, P., & Okpalugo, T. I. T. (2006). Raman study of multiwalled carbon nanotubes functionalized with oxygen groups. *Journal of Vacuum Science & Technology B: Microelectronics and Nanometer Structures*, *24*(2), 715. doi:10.1116/1.2180257

(40) Osswald, S., Flahaut, E., Ye, H., & Gogotsi, Y. (2005). Elimination of D-band in Raman spectra of double-wall carbon nanotubes by oxidation. *Chemical Physics Letters*, *402*(4-6), 422–427. doi:10.1016/j.cplett.2004.12.066

(41) DiLeo, R. A., Landi, B. J., & Raffaelle, R. P. (2007). Purity assessment of multiwalled carbon nanotubes by Raman spectroscopy. *Journal of Applied Physics*, *101*(6), 064307. doi:10.1063/1.2712152

(42) Lee, S., Peng, J.-W., & Liu, C.-H. (2009). Probing plasma-induced defect formation and oxidation in carbon nanotubes by Raman dispersion spectroscopy. *Carbon*, *47*(15), 3488–3497. doi:10.1016/j.carbon.2009.08.019

(43) Menéndez, J. A., Arenillas, A., Fidalgo, B., Fernández, Y., Zubizarreta, L., Calvo, E. G., & Bermúdez, J. M. (2010). Microwave heating processes involving carbon materials. *Fuel Processing Technology*, *91*(1), 1–8. doi:10.1016/j.fuproc.2009.08.021

(44) Haque, K. E. (1999). Microwave energy for mineral treatment processes—a brief review. *International Journal of Mineral Processing*, *57*(1), 1–24. doi:10.1016/s0301-7516(99)00009-5

(45) Paton, K. R., & Windle, A. H. (2008). Efficient microwave energy absorption by carbon nanotubes. *Carbon*, *46*(14), 1935–1941. doi:10.1016/j.carbon.2008.08.001

(46) Zlotorzynski, A. (1995). The Application of Microwave Radiation to Analytical and Environmental Chemistry. *Critical Reviews in Analytical Chemistry*, *25*(1), 43–76. doi:10.1080/10408349508050557

(47) Irin, F., Shrestha, B., Cañas, J. E., Saed, M. A., & Green, M. J. (2012). Detection of carbon nanotubes in biological samples through microwave-induced heating. *Carbon*, *50*(12), 4441–4449. doi:10.1016/j.carbon.2012.05.022

(48) Wang, L., & Dang, Z.-M. (2005). Carbon nanotube composites with high dielectric constant at low percolation threshold. *Applied Physics Letters*, *87*(4), 042903. doi:10.1063/1.1996842

(49) Li, Y.-H., & Lue, J.-T. (2007). Dielectric Constants of Single-Wall Carbon Nanotubes at Various Frequencies. *Journal of Nanoscience and Nanotechnology*, *7*(9), 3185–3188. doi:10.1166/jnn.2007.658

(50) Vázquez, E., & Prato, M. (2009). Carbon Nanotubes and Microwaves: Interactions, Responses, and Applications. *ACS Nano*, *3*(12), 3819–3824. doi:10.1021/nn901604j

(51) Mashal, A., Sitharaman, B., Xu Li, Avti, P. K., Sahakian, A. V., Booske, J. H., & Hagness, S. C. (2010). Toward Carbon-Nanotube-Based Theranostic Agents for Microwave Detection and Treatment of Breast Cancer: Enhanced Dielectric and Heating Response of Tissue-Mimicking Materials. *IEEE Transactions on Biomedical Engineering*, *57*(8), 1831–1834. doi:10.1109/tbme.2010.2042597

(52) Imholt, T. J., Dyke, C. A., Hasslacher, B., Perez, J. M., Price, D. W., Roberts, J. A., … Tour, J. M. (2003). Nanotubes in Microwave Fields: Light Emission, Intense Heat, Outgassing, and Reconstruction. *Chemistry of Materials*, *15*(21), 3969–3970. doi:10.1021/cm034530g

(53) Odom, M. G. B., Sweeney, C. B., Parviz, D., Sill, L. P., Saed, M. A., & Green, M. J. (2017). Rapid curing and additive manufacturing of thermoset systems using scanning microwave heating of carbon nanotube/epoxy composites. *Carbon, 120*, 447–453. doi:10.1016/j.carbon.2017.05.063

(54) Sweeney, C. B., Lackey, B. A., Pospisil, M. J., Achee, T. C., Hicks, V. K., Moran, A. G., … Green, M. J. (2017). Welding of 3D-printed carbon nanotube–polymer composites by locally induced microwave heating. *Science Advances*, *3*(6), e1700262. doi:10.1126/sciadv.1700262

(55) MacKenzie, K., Dunens, O., & Harris, A. T. (2009). A review of carbon nanotube purification by microwave assisted acid digestion. *Separation and Purification Technology*, *66*(2), 209–222. doi:10.1016/j.seppur.2009.01.017

(56) Priya, B. R., & Byrne, H. J. (2009). Quantitative Analyses of Microwave-Treated HiPco Carbon Nanotubes Using Absorption and Raman Spectroscopy. *Journal of Physical Chemistry C*, *113*(17), 7134–7138. doi:10.1021/jp808913x

(57) Shim, H. C., Song, J.-W., Kwak, Y. K., Kim, S., & Han, C.-S. (2009). Preferential elimination of metallic single-walled carbon nanotubes using microwave irradiation. *Nanotechnology, 20*(6), 065707. doi:10.1088/0957-4484/20/6/065707

(58) Sanchez, V. C., Pietruska, J. R., Miselis, N. R., Hurt, R. H., & Kane, A. B. (2009). Biopersistence and potential adverse health impacts of fibrous nanomaterials: what have we learned from asbestos? *Wiley Interdisciplinary Reviews: Nanomedicine and Nanobiotechnology, 1*(5), 511–529. doi:10.1002/wnan.41

(59) Firme, C. P., & Bandaru, P. R. (2010). Toxicity issues in the application of carbon nanotubes to biological systems. *Nanomedicine: Nanotechnology, Biology and Medicine*, *6*(2), 245–256. doi:10.1016/j.nano.2009.07.003

(60) Li, S., Irin, F., Atore, F. O., Green, M. J., & Cañas-Carrell, J. E. (2013). Determination of multi-walled carbon nanotube bioaccumulation in earthworms measured by a microwave-based detection technique. *Science of The Total Environment,* 445-446, 9–13. doi:10.1016/j.scitotenv.2012.12.037

(61) Saleh, N. B., Pfefferle, L. D., & Elimelech, M. (2008). Aggregation Kinetics of Multiwalled Carbon Nanotubes in Aquatic Systems: Measurements and Environmental Implications. *Environmental Science & Technology*. *42,* 7963-7969. doi:10.1021/es801251c

(62) Sano, M., Okamura, J., & Shinkai, S. (2001). Colloidal Nature of Single-Walled Carbon Nanotubes in Electrolyte Solution: The Schulze-Hardy Rule. *Langmuir*, *17*, 7172-7173. doi: 10.1021/la010698+

(63) Jiang, L., Gao, L., & Sun, J. (2003). Production of aqueous colloidal dispersions of carbon nanotubes. *Journal of Colloid and Interface Science*, *260*(1), 89–94. doi:10.1016/s0021-9797(02)00176-5

(64) Lisunova, M. O., Lebovka, N. I., Melezhyk, O. V., & Boiko, Y. P. (2006). Stability of the aqueous suspensions of nanotubes in the presence of nonionic surfactant. *Journal of Colloid and Interface Science*, *299*(2), 740–746. doi:10.1016/j.jcis.2006.03.012

(65) Jung, D.-H., Koan Ko, Y., & Jung, H.-T. (2004). Aggregation behavior of chemically attached poly(ethylene glycol) to single-walled carbon nanotubes (SWNTs) ropes. *Materials Science and Engineering: C*, *24*(1-2), 117–121. doi:10.1016/j.msec.2003.09.006

(66) Rowles III, L. S. (2015). *Sustained Release of Silver Ions for Disinfection: Merging Century Old Navajo Pottery Techniques with Novel Nanomaterials* (Unpublished Report). The University of Texas at Austin, Austin, TX.

(67) Mahajan, A., Kingon, A., Kukovecz, Á., Konya, Z., & Vilarinho, P. M. (2013). Studies on the thermal decomposition of multiwall carbon nanotubes under different atmospheres. *Materials Letters*, *90*, 165–168. doi:10.1016/j.matlet.2012.08.120

(68) Hsieh, Y.-C., Chou, Y.-C., Lin, C.-P., Hsieh, T.-F., & Shu, C.-M. (2010). Thermal Analysis of Multi-walled Carbon Nanotubes by Kissinger's Corrected Kinetic Equation. *Aerosol and Air Quality Research*, *10*(3), 212–218. doi:10.4209/aaqr.2009.08.0053

Vita

Sneha Siddharth Jain is a Texas transplant, living in the Dallas area. In 2014, Sneha began her studies at The University of Texas at Austin as an undergraduate. She will graduate in May 2019 with a B.S. in Chemical Engineering Honors and B.A. in Plan II Honors, Economics, and Russian, East European, & Eurasian Studies. During her undergraduate career, Sneha joined Dr. Navid Saleh's Sustainable Nano-Engineering for Water Treatment Lab and worked with Dr. Dipesh Das in synthesizing, characterizing, and evaluating the behavior of nanomaterial hybrids. In fall 2017, she began independent work in the incorporation of carbon nanotubes in point-of-use bacterial inactivation devices for water treatment.

Throughout this process, Sneha is thankful and appreciative of the support of Dr. Saleh, her lab mates, her family, and her friends.

Email address: SnehaJain@utexas.edu

This thesis was typed by the author.